Ceramics International 49 (2023) 22566–22575

Contents lists available at ScienceDirect

Ceramics International

journal homepage: www.elsevier.com/locate/ceramint

Enhanced magnetostriction of Co–Ni-ferrite composites derived from hard ($CoFe_2O_4$) and soft ($NiFe_2O_4$) magnetostrictive phases

Satish M [a], H.M. Shashanka [a], S. Saha [b], P.N. Anantharamaiah [a,*], C.V. Ramana [c,d,**]

[a] Department of Chemistry, Faculty of Mathematical and Physical Sciences, M. S. Ramaiah University of Applied Sciences, Bangalore, 560058, India
[b] Department of Materials Engineering, Indian Institute of Science, Bangalore, 560012, India
[c] Center for Advanced Materials Research, University of Texas at El Paso, 500 W. Univ. Ave., El Paso, TX, 79968, USA
[d] Department of Mechanical Engineering, University of Texas at El Paso, 500 W. Univ. Ave., El Paso, TX, 79968, USA

ARTICLE INFO

Handling Editor: Dr P. Vincenzini

Keywords:
Spinel ferrites
Composites
Nanomaterials
Magnetic properties
Magnetostriction
Sensors

ABSTRACT

We report on the enhanced magnetostrictive characteristics of composites derived from the hard cobalt ferrite ($CoFe_2O_4$; CFO) and soft nickel ferrite ($NiFe_2O_4$; NFO) materials. The CFO, NFO and CFO-NFO (CNFO) mixed composites (25NFO + 75CFO, 50NFO + 50CFO and 75NFO + 25 CFO) were synthesized by employing a cost-effective and eco-friendly glycine-nitrate autocombustion method. The CFO, NFO and their mixed composites were evaluated to assess their phase purity, surface morphology, magnetic properties, and magnetostrictive characteristics. The X-ray diffraction (XRD) and electron microscopy analyses revealed that the CFO and NFO nanomaterials were phase pure, porous in nature, and nano-sized with average crystallite size of 73 nm (CFO) and 69 nm (NFO). Subsequently, the Co–Ni-ferrite composite made from CFO and NFO in equal quantity by sintering at 1200 °C indicate that the lattice parameter, *a*, of the composite lies in between the lattice parameters of respective components (CFO-8.390 Å and NFO-8.343 Å) indicating that both phases co-exists as single-phase in the composite. The grains of the sintered compounds are nearly spherical shape with the average sizes ~670 nm, ~550 nm and ~560 nm, respectively, for CFO, NFO and 50NFO +50CFO composite. Due to grain growth upon sintering, magnetizations of the sintered CFO and NFO nanomaterials are higher than that of as-synthesized samples. Interestingly, the magnetization curves of sintered CNFO composites exhibit symmetric nature (single loop), where their magnetization lies in between the magnetizations of NFO and CFO phases, indicating a proper exchange coupled between the two phases. The composites demonstrate better magnetostriction at lower magnetic fields than the parent sintered CFO and NFO samples. At an applied magnetic field of 2 kOe, the obtained magnetostriction value for 50NFO +50CFO composite (−120 ppm) is nearly 500% higher than that of CFO (−20 ppm) and 300% higher than that of NFO (−30 ppm). The structure-phase-property correlation established in these composites expected to provide a road-map for their possible applications in electromagnetic devices.

1. Introduction

Cubic spinel-type ferrites with a general formula MFe_2O_4 (M is divalent metal ions) received immense attention among the scientists and researchers owing to their tunable structural, magnetic, electrical, optical and catalytic properties [1–5]. Due to their attractive properties, ferrite systems find numerous applications in the fields of data storage, magnetic hyperthermia, photo- and electro-catalysis, sensors, permanent magnets, EMI shielding, etc [6–11]. Although nickel ferrite ($NiFe_2O_4$; NFO) and cobalt ferrite ($CoFe_2O_4$) belong to cubic spinel-type ferrite system, they demonstrate different magnetic properties; $NiFe_2O_4$ (NFO) is soft-magnetic phase whereas $CoFe_2O_4$ (CFO) is hard magnetic phase. The presence of highly anisotropic Co^{2+} ions at the octahedral interstitial sites (B-site in general AB_2O_4 spinel structure) makes the CFO as magnetically hard phase [12].

CFO is a traditionally known functional magnetic material, which finds numerous applications in high density magnetic recording media and related device applications, thanks to its high saturation magnetization (~80 emu/g) and high coercivity (~5400 Oe) [13,14]. CFO not only displays beneficial magnetic properties, but also unveils decent

* Corresponding author.
** Corresponding author. Center for Advanced Materials Research, University of Texas at El Paso, 500 W. Univ. Ave., El Paso, TX, 79968, USA..
E-mail addresses: anantharamaiah.cy.mp@msruas.ac.in (P.N. Anantharamaiah), rvchintalapalle@utep.edu (C.V. Ramana).

https://doi.org/10.1016/j.ceramint.2023.04.093
Received 3 February 2023; Received in revised form 3 April 2023; Accepted 13 April 2023
Available online 20 April 2023

chemical and mechanical stabilities, especially the high corrosion resistance, high thermal stability etc. [14]. Structurally, CFO has been recognized as mixed spinel-type FCC structure with two distinct voids viz, tetrahedral (A) and octahedral (B), and these voids are occupied randomly by Fe^{3+} and Co^{2+} [15]. For CFO, *[100]* and *[111]* crystallographic directions are the easy and hard magnetization axes, respectively [15]. The magnetic properties of CFO are sensitive to microstructural aspects and hence the properties would be different for nano, bulk and thin film $CoFe_2O_4$ [14,16–18]. In fact, the ability to tune the material properties by means of controlling the structure, phase, and dopant concentration etc., made CFO and CFO-composites as attractive candidate materials for many of the magnetic, electrochemical and sensor applications.

In the family of MF_2O_4 type materials, CFO and NFO have been widely considered for sensor applications in magneto-mechanical and electro-mechanical systems. Both CFO and NFO are well-known for their magnetostriction (λ) strain at room temperature, but magnitudes of λ are different for both phases [19–23]. The reported $\lambda_{max}\lambda_{max}$ for sintered polycrystalline CFO varies from ∽-100 ppm to ∽-400ppm along the parallel direction ($\lambda_{||}$) [3–12,19–21] and that for NFO reported as −25ppm to −40 ppm [22,23]. These values depend on numerous factors [1–12,19–21], such as synthetic conditions adopted for materials processing, microstructure, method of synthesis, chemical environment etc., which also determine the performance characteristics.

Due to superior magnetostrictive properties of CFO and NFO, they have been employed as magnetostrictive component in designing magnetoelectric composite materials [24,25]. Strong spin-orbit coupling due to Co^{2+} at the B-sites makes CFO, in addition to hard magnetic nature, to attain a high degree of magnetostriction than that possessed by NFO. High-magnetostriction relatively at high magnetic fields limits CFO use for sensor applications, in particular for torque sensors. However, it is shown in the literature ways to tune the magnetostriction strain of cobalt ferrite towards lower magnetic fields by performing magnetic field annealing and substitution by suitable metal ions (Bi, Mn, Al, Ga, Zn, In, Mg) [19,26–31]. Apart from these considerations, the scientific and engineering community continuously exploring the new and/or alternative routes to enhance the magnetostriction performance of the materials at lower magnetic fields. The concept of nanocomposite is one among the relatively new and attractive method being explored in designing materials for various applications, specifically the field of electromagnetics. Additionally, among the general classification of nanocomposites for electromagnetics, composites which can integrate the hard and soft magnetic phases into a single platform is gaining tremendous importance in order to obtain materials with tunable properties and enhanced performance, which is otherwise not possible.

In the early 1990s, Kneller and Hawig conceptualized exchange-spring mechanism in order to accomplish high energy product $(BH)_{max}$ in a nanocomposite comprising of hard and soft magnetic phases [32]. The authors projected that composite materials made of two appropriately dispersed ferromagnetic and mutually exchange-coupled phases (one is hard magnetic phase in order to have a high H_C, while other must be a soft magnetic phase just providing a high saturation M_S) can be employed as permanent magnets [32]. Thus, based on the exchange spring concept, if both soft and hard magnetic phases in a composite are adequately exchange-coupled with each other, then the composite is regarded as an exchange spring magnet. Using this concept, Roy et al. reported nearly 13% enhancement of $(BH)_{max}$ after making a nanocomposite between Fe_3O_4 (soft phase) and $BaCa_2Fe_{16}O_{27}$ (hard phase) phases [33]. The high saturation magnetization of the soft phase and the high coercivity of the hard phase are utilized for superior magnetic property of the composite compared to the individual soft and hard phases, thus providing high magnetic energy product [33]. Realizing the significant benefits and potential of the approach, in recent years, various composites made of soft and hard phases, such as $Fe_3O_4/CoFe_2O_4$, $CoFe_2O_4/SrFe_{12}O_{19}$, $CoFe_2O_4/BaFe_{12}O_{19}$, $Co_{0.8}Ni_{02}Fe_2O_4/SrFe_{10}Al_2O_{19}$, $CoFe_2O_4/FeCo$, $NiFe_2O_4/BaFe_{12}O_{19}$ etc., were studied to improve/enhance the magnetic parameters through the exchange-spring concept [34–40].

Based on the concept of exchange-spring mechanism, we developed an approach to enhance the magnetostriction at lower magnetic fields which is expected to tremendously benefit the field of magnetic, torque, and electromagnetic sensors for aerospace and energy technologies. The approach is based on making an appropriate composites between hard-magnetostrictive phase (CFO) and soft magnetostrictive phase (NFO) through the concept of exchange-spring mechanism, where there is no need for any special processing or doping or metal-ion substitution into CFO or NFO. Also, compared to previous efforts towards realizing a composite from structurally two different material systems, the CFO + NFO composites being derived from the simple and the family of isostructural and composition-equivalent spinel structured metal-ferrites (MFe_2O_4) may open up new avenues to design materials for electromagnetic device applications. Note that, CFO is regarded as hard-magnetostrictive phase as it shows high magnetostriction at higher magnetic field whereas NFO exhibits high magnetostriction at lower magnetic field and hence the soft-magnetostrictive phase. Moreover, CFO and NFO are magnetically hard and soft phases, respectively. Furthermore, the magnetostrictive properties of composites between CFO and NFO are yet to be explored; therefore, in the present work, we made an attempt to investigate such composites deeply and to understand their fundamental structure-composition-property correlation. As presented and discussed in the paper, the results demonstrate that the composites exhibit enhanced magnetostriction at lower magnetic fields against the individual components of the composite.

2. Experimental details

2.1. Synthesis of CFO and NFO nanomaterials

All the materials in this work were synthesized using the well-known autocombustion method. Consideration of autocombustion method over other wet-chemical synthesis methods is due to the fact that, it is simple, inexpensive, fast, and one-step synthesis [41]. Moreover, large quality of sample in single phase nanostructure could be attained using the autocombustion method [41]. Thus, adequate amounts of $CoFe_2O_4$ and $NiFe_2O_4$ nanomaterials were synthesized using a solution-based autocombustion method [26], where glycine employed as a fuel. Metal nitrates, such as nickel nitrate ($Ni(NO_3)_2$ $6H_2O$), cobalt nitrate ($Co(NO_3)_2$ $6H_2O$) and ferric nitrate ($Fe(NO_3)_3$ $9H_2O$), all are in analytical grade with purity ∼99%, were used as source materials. The nitrate ions associated with the metal salts serve as oxygen source for combustion process. Initially, metal nitrates, weighed according to the ratio of chemical formulas, were transferred into crystallizing dish (100 ml) and dissolved with a known volume of distilled water (20 ml), followed by high-frequency sonication for a few minutes to make homogeneity. In a separate beaker of 50 ml, glycine crystals (1 mol per mole of metal ion) were taken and made solution with distilled water. The glycine solution was then mixed with the metal nitrates solution and sonicated. It is observed that after mixing the glycine solution with that of the metal nitrate solution, solution color changed from the wine red to dark wine red owing to the formation of metal ions-glycine complexes. To initiate the combustion process, the resultant solution was then placed on a pre-heated hot plate by maintaining a temperature of 200 °C. When more than 90% of water molecules removed from the solution, the solution became highly viscus and brown colored fumes (oxides of nitrogen) began to expel. Subsequently, a quick auto-ignition took place leading to highly porous ferrite powders. The resultant ferrite powders pulverized into fine powders and subjected to phase purity analysis and morphology investigation.

As-synthesized ferrite powders were molded into disc-shaped pellets (thickness ∼ 3 mm and diameter ∼ 12 mm) by applying 40 bar pressure. These pellets were then sintered at elevated temperature (1200 °C) for 2 h with a heating rate of 5 °C per minute and furnace cooled. Two pellets

for each sample were made; one was used for structural, magnetic and morphology characterization, and the other for magnetostriction measurements. For better comparison and correlation, all the ferrite pellets were processed under the same conditions. It has been noted that, upon sintering, the ferrite pellets shrink considerably due to densification through grain growth.

2.2. Synthesis of NFO + CFO composites

CFO and NFO mixed composites synthesized with variable composition. Three different composites (75NFO + 25CFO, 50NFO + 50CFO and 25NFO + 75CFO) were prepared by taking proper wt% of individual component of the composite. The calculated amounts of as-synthesized NFO and CFO nanopowders were weighed according to wt% into agate mortar and mixed homogeneously using acetone solvent (mixing medium). Afterwards, a few drops of 2% PVA solution was added to homogeneously mixed ferrite powders and ground meticulously to bind the particles firmly, and then molded as disc-shaped pellet. The green pellets heated to 1200 °C with heating rate of 5 °C per min and sintered at the same temperature for 2 h, and furnace cooled. Here also, similar to the individual compositions of CFO and NFO, two pellets for each composite were made for respective characterizations and also to compare with individual hard and soft magnetic component materials.

2.3. Characterization

The crystal structure and phase analyses of the as synthesized CFO and NFO nanomaterials, CFO and NFO sintered ceramic materials, and CNFO composites was made by means the X-ray diffraction (XRD) measurements. For XRD measurements, SmartLab, Rigaku X-ray diffractometer equipped with Cu Kα X-ray source was employed. Slow-scan XRD powder data of as-synthesized NFO, CFO samples and the sintered NFO, CFO and the NFO + CFO composites samples were recorded in 2θ range of 10° - 80° with a step-size of 0.01°. To investigate the surface morphology, scanning electron microscopy measurements were made Using Quanta 200, FEI scanning electron microscopy (SEM). All of the as-synthesized ferrite powders and the sintered samples were investigated. The sintered pellets were broken and SEM images of inner regions of sintered specimen were captured at different scale and magnification. The magnetic properties of the as-synthesized NFO, CFO samples and the sintered NFO and CFO and NFO + CFO composites samples were investigated by recording their room temperature magnetization hysteresis loops in the field region −20 kOe ≤ H ≤ 20 kOe with a step size of 50 Oe using a lakeshore vibrating sample magnetometer. To find out magnetic phase transition temperature (Curie temperature) of the sintered CFO, NFO and the NFO + CFO composite samples, their thermomagnetic curves were recorded at a constant magnetic field of 100 Oe. For magnetostriction measurements, strain gauge of resistance 350 Ω has been glued on the surface of sintered pellet using cyanoacrylate adhesive, and cured at ~85 °C for a few hours. The magnetostriction strain curves of the samples were measured at room temperature along the direction parallel to applied magnetic field (−8 kOe ≤ H ≤ +8 kOe).

3. Results and discussion

3.1. Studies on as-synthesized CFO and NFO samples

3.1.1. X-ray diffraction (XRD)

The crystal structure and phase analyses first directed towards the as-synthesized CFO and NFO samples. The XRD data of as-synthesized CFO and NFO nanomaterials are shown in Fig. 1. The XRD patterns (Fig. 1a) exhibit the presence of peaks, which are well-resolved with good signal to noise ratio. The Bragg's reflections (220), (311), (222), (400), (422), (511), and (440) situated at diffraction angles of 2θ ~ 30.26°, 35.65°, 37.29°, 43.33°, 53.78°, 57.33° and 62.95°, respectively, are the characteristics peaks of the cubic spinel ferrites crystallizing in $Fd\bar{3}m$ space group. Thus, the XRD data confirm that both CFO and NFO crystallize in cubic spinel structure. Furthermore, no other reflections pertaining to impurity phase/s found in the XRD profiles of both samples demonstrate that as-synthesized CFO and NFO ferrite nanomaterials are phase pure. However, the broader nature of the peaks in the XRD suggests that both Co- and Ni-ferrite powders are nanocrystalline. Coupled with nanocrystalline nature, the uniform or non-uniform microstrain developed inside the CFO and NFO nanomaterials could be one of factors for the broad peaks observed in XRD. Previously, Ramana et al. demonstrated that the XRD peak broadening occurs in nanocrystalline materials due to size-reduction as well as microstrain [42,43]. In fact, such size-strain

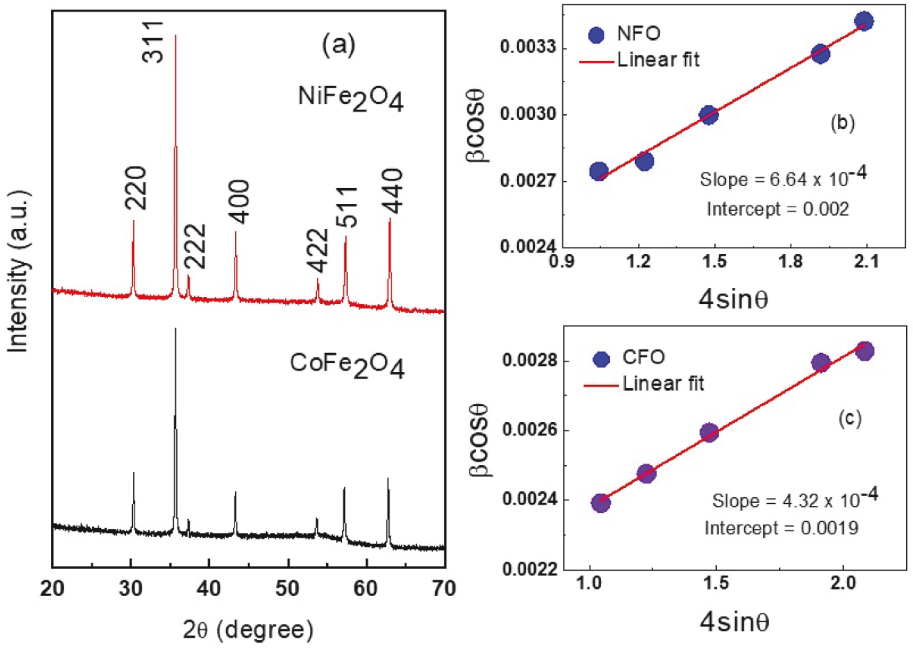

Fig. 1. (a) X-ray diffraction data of as-synthesized CFO and NFO nanomaterials; (b,c) the Williamson-Hall plots for NFO and CFO samples, respectively.

coupled effect can be predominant in simple and multi-component oxides. It is, therefore, important to perform detailed analyses about the 'size and strain' in order derive reliable information about the CFO and NFO nanomaterials. Therefore, further analyses were made using Williamson-Hall method, which is quite useful to evaluate the average crystallite size and average strain in the as-synthesized CFO and NFO nanomaterials.

According to Williamson-Hall analysis [44], relation between line width, crystallite size and microstrain is represented by following relations:

$$\beta \cos\theta = \frac{K\lambda}{D_v} + 4\varepsilon_{str} \sin\theta \quad (1)$$

for a Lorentzian peak profile function

$$\beta^2 \cos^2\theta = \left(\frac{K\lambda}{D_v}\right)^2 + 16\varepsilon_{str}^2 \sin^2\theta \quad (2)$$

for a Gaussian peak profile function

where ε_{str} is weighted average strain, β is the full width at half maximum intensity of a peaks in radian, K is a particle shape factor (0.9 for spherical), D_v is the average crystallite size, λ is the wavelength of the X-ray source used and θ is the Bragg's diffraction angle. Relatively good fit observed when Lorentian peak profile function was used to fit individual peaks of the CFO and NFO samples. Therefore, equation (1) has been adopted in the analyses. The plots of βcosθ *versus* 4sinθ for the NFO and CFO samples are shown in Fig. 1b and c, respectively. The data points were fitted with a linear function. From the slope and intercept values, strain and crystallite size of the ferrite samples were deduced and the resultant values are listed in Table 1. The structural parameter (lattice parameter) 'a' and theoretical density (ρ) of the samples were estimated using the formulae [45], for cubic crystal system, given below:

$$a = d_{hkl}\sqrt{h^2 + k^2 + l^2} \ldots\ldots (3)$$

$$\rho_{theor} = \frac{ZM}{N_A a^3} \left(\frac{g}{cm^3}\right) \ldots\ldots (4)$$

where d_{hkl} is the distance between the crystal planes (interplanar distance), *hkl* are Miller indices, Z is number of molecules per unit cell (8 molecules for cubic spinel), M is molecular mass and N_A is Avogadro's number (6.023×10^{23} molecules per gram). The lattice parameter and theoretical density (ρ) of the samples are listed in Table 1, and found no large changes in the values between two ferrite systems.

3.1.2. Surface morphology – scanning electron microscopy

The SEM images of as-synthesized CFO and NFO samples are presented in Fig. 2. It is evident from the images that it is extremely difficult to figure out individual ferrite particles because the ferrite particles are nanosized and are agglomerated into clusters of irregular shaped, probably due to their magnetic interactions and high surface energies. In fact, such agglomeration, especially at the nanoscale dimensions, is seen in a variety of ferrites samples as widely documented in the literature. Moreover, the ferrite powders exhibit porous structure. The porous structure could be certainly ascribed to formation and release of voluminous gases such as oxides of carbon, nitrogen, etc., during autocombustion process.

Table 1
Average crystallite size (D_v), strain (ε), lattice parameter (a) and theoretical density (ρ) of the as-synthesized NFO and CFO samples.

Sample	'D_v' (nm) (±1)	ε_{strain} x 10^{-4} (±0.02 × 10^{-4})	'a' (Å) (±0.002)	$\rho_{theor.}$ (g/cm^3) (±0.02)
NFO	69	6.64	8.345	5.35
CFO	73	4.32	8.348	5.35

3.1.3. Magnetic properties

To assess the magnetic nature of the as-synthesized spinel ferrite powders, room temperature magnetization (M verses H) hysteresis loops were recorded in the magnetic field region of -20 kOe $\leq H \leq +20$ kOe. The M − H data of CFO and NFO nanomaterials are displayed in Fig. 3. Although the synthesized ferrite powders are nanosized, both samples demonstrate a lucid hysteresis loop owing to the ferrimagnetic nature of the samples. It is evident (Fig. 3a) that area under the loop of the CFO sample is remarkably larger than that observed for the NFO sample. As expected, larger loop area signifies hard magnetic nature of CFO, whereas smaller loop area indicates soft magnetic nature of the NFO. Important magnetic parameters (saturation magnetization (M_S), coercivity (H_c), anisotropy constant (K_1)), which extracted from the magnetization curves, of CFO and NFO nanomaterials are listed in Table 2. Herein, Law of approach to saturation (LAS) method has been employed to compute values of M_S, K_1 of the samples.

According to LAS, magnetization (M) of the magnetic material as a function of applied magnetic field (H) is expressed as [26]:

$$M = M_s - \frac{8K_1^2}{105H^2M_s} \quad (5)$$

Where the numerical coefficient 8/105 is pertaining to polycrystalline samples with cubic anisotropy and K_1 is the first order magneto-crystalline anisotropy constant. The magnetization of the samples at high magnetic fields ($H \gg H_C$) has been used to fit for LAS. The linear fit to the LAS for CFO and NFO is shown in Fig. 3b and c, respectively. M_S and K_1 values of the samples obtained in the present study are comparable with the reported values [46,47] for similar particle sizes. In fact, the magnetocrystalline anisotropy constant of CFO is significantly higher than that of NFO which is due to its hard magnetic nature and the presence of highly anisotropic Co^{2+} at the octahedral site. The values of M_S, H_c and K_1 of as-synthesized CFO and NFO are listed in Table 2.

3.2. Studies on sintered CFO and NFO materials and CFO + NFO composites

3.2.1. X-ray diffraction (XRD) analysis

The XRD data of NFO, CFO and 50NFO + 50CFO composite sintered at 1200 °C are presented in Fig. 4. Similar to as-synthesized samples, the sintered samples also exhibit the presence of well-resolved and intense peaks indicating the crystalline nature of the samples. Here also the peaks due to spinel cubic ferrites appear and the data (Fig. 4a) confirm that the CFO, NFO and 50NFO+ 50CFO composite crystallize in the cubic spinel structure with a phase purity well maintained. It can be noted that the X-ray diffraction peaks are rather sharp and highly intense compared that of as-synthesized samples. This is due to significant grain growth induced by the temperature of sintering. In fact, the sharp and intense peaks help to determine the precise position of the peaks in the slow scans. Such a slow scan for the enlarged view of (311) peak is shown in Fig. 4b, where the relative peak shift is evident. The peak position for NFO is positioned at a higher diffraction angle compared to that of CFO suggesting that the unit cell parameter of NFO is lower than that of CFO. The unit cell parameters determined for NFO and CFO are 8.343 and 8.390 Å, respectively. These values are comparable with the sintered ferrite samples, as reported in the literature [22,26]. Interestingly, as evident from Fig. 4b, the peak position for the 50NFO +50CFO composite is positioned in between the CFO and NFO samples. This suggests that both hard-CFO and soft-NFO phases co-exists as a single entity in composite.

3.2.2. Microstructural analysis

The SEM images of the sintered NFO, CFO and 50NFO+ 50CFO composite samples are shown in Fig. 5 (top panel). Unlike particles of

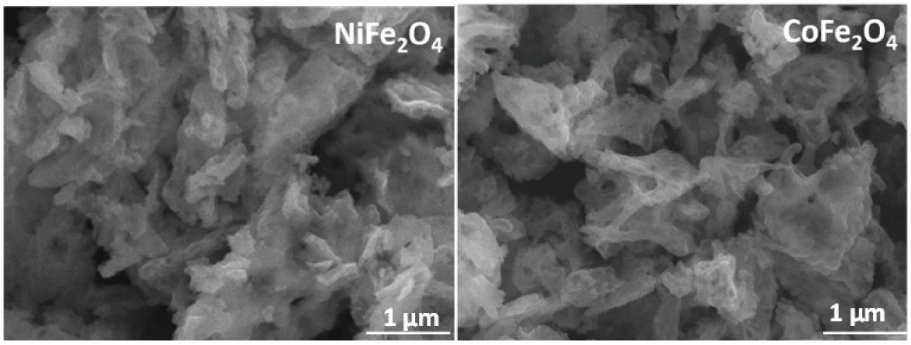

Fig. 2. SEM images as-synthesized NFO and CFO samples.

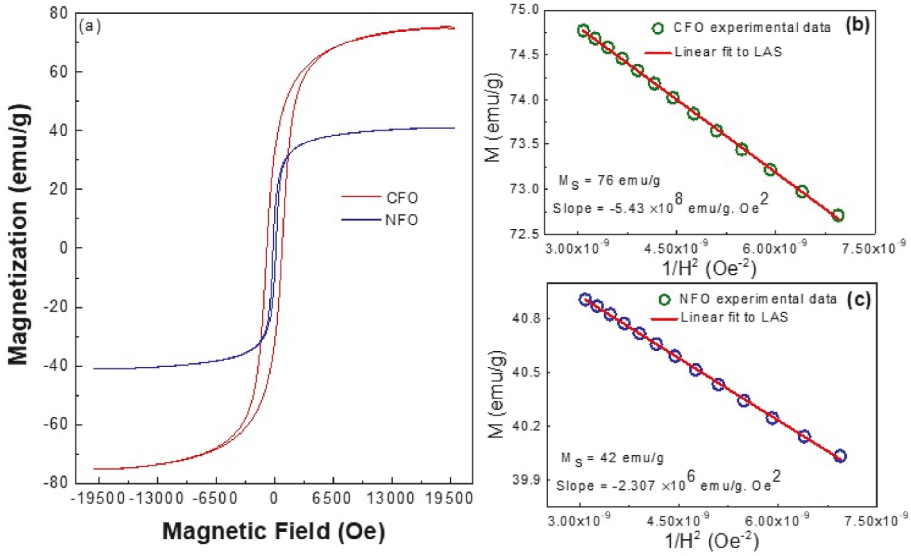

Fig. 3. (a) Magnetic field-dependant magnetization curves of as-synthesized CFO and NFO; (b,c) linear fit to LAS for CFO and NFO samples, respectively.

Table 2
Magnetic parameters of as-synthesized NFO and CFO samples.

Sample	M_s (emu/g) (±1)	H_c (Oe) (±1)	M_r (emu/g) (±1)	Slope (±0.01 × 10^8)	k_1 x10^6 (erg/cm^3) (0.01 × 10^6)
CFO	76	852	33	−5.43 × 10^8	3.8
NFO	42	166	10	−2.307 × 10^6	0.19

the as-synthesized samples, ferrite grains in the sintered samples are evidently distinguishable and are in nanosized. Even after sintering at 1200 °C, size of the ferrite grains in all three samples is less than a micron. From the SEM images, individual grains of the samples were measured using digital microgram software. The corresponding grain size histograms generated are shown in Fig. 5 (bottom panel). Nearly uniform grain size can be seen in the SEM image of NFO sample, where the size of ferrite grains ranging from ∽400 to ∽800 nm, with a mean size of 550 nm. In case of CFO sample, a wide range of grain size can be seen. The grains are as smaller as 400 nm and as larger as 1 µm, while CFO-grains with a mean grain size of ∽670 nm are evident. In addition, majority of the CFO grains are in spherical morphology. Only a few of them are in irregular shape. Such morphology, and specifically shape, expected to show significant effects on the magnetic parameters, particularly H_C, of the samples [5]. Similar morphology features, particularly the presence of smaller and larger ferrite grains, can be observed in the SEM image of 50NFO+ 50CFO composite sample, with the mean size of 560 nm. Another important observation from the SEM images that both NFO and 50NFO+ 50CFO composite illustrate high degree of packing with less intergranular porosity, whereas CFO sample shows high porosity with less packing between the grains.

3.2.3. *Magnetic properties*

Room temperature field-dependant magnetization hysteresis loops for the sintered CFO, NFO and NFO + CFO composites are shown in Fig. 6. Noticeable change in magnetic parameters of both CFO and NFO samples has been observed after sintering the nano ferrite powders at higher temperature (1200 °C). H_C of the sintered samples measured directly from the M-H curves, whereas M_S and K_1 values were estimated by interpreting the M-H curves through the method of LAS, as discussed in the earlier section. Linear fit to M vs $1/H^2$ data for the NFO, CFO and composites are shown in Fig. 7. The obtained values of H_C, M_S, K_1 of the sintered samples are enlisted in Table 3. After sintering NFO sample from its nanopowders, M_S and K_1 values increased from 42 emu/g to 47 emu/g and 0.19 × 10^{+6} erg/cm^3 to 0.8 × 10^{+6} erg/cm^3, respectively, whereas H_C decreased from 166 to 56 Oe. The increased M_S and decreased H_C with sintering temperature is certainly attributed to grain growth that suppresses the magnetic dead layer on the ferrite

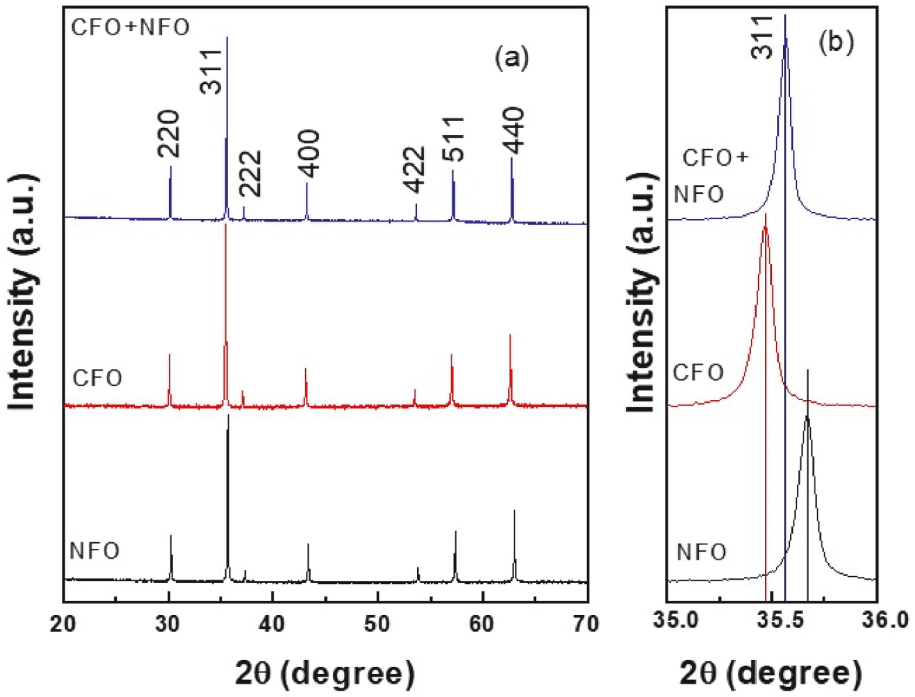

Fig. 4. (a) XRD patterns of sintered NFO, CFO and 50NFO+ 50CFO composite samples; (b) the slow XRD scans in $35 \leq 2\theta \leq 36$ region highlighting the relative (311) peak shift in CFO and NFO materials, and 50CFO+ 50NFO composite.

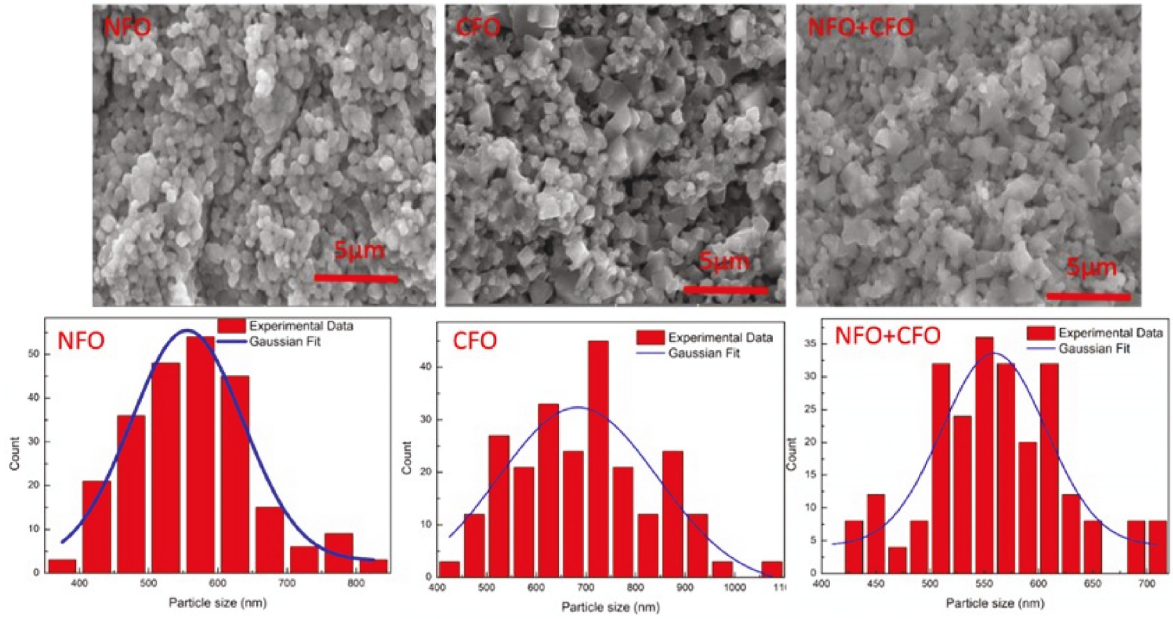

Fig. 5. SEM images of sintered NFO, CFO and 50 NFO+ 50 CFO composites samples, shown in 5 μm scale. The corresponding histograms of grain size distribution are shown just below the SEM images of the samples.

nanoparticles and make the system magnetically softer.

Similar to NFO sample, M_S and K_1 values of CFO sample increased from 76 emu/g to 81 emu/g and 3.8×10^6 erg/cm^3 to 4.44×10^6 erg/cm^3, respectively. Interestingly, unlike NFO specimen, H_C of CFO specimen increased from 852 Oe to 1094 Oe, despite the fact that the ferrite particle size increased from 73 nm to 670 nm. The increase of H_C is probably due to microstructural change (smaller and larger grains with irregular shape), as revealed from the SEM imaging analysis. Magnetic parameters of sintered CFO sample are significantly higher than that observed for NFO sample due to its hard magnetic nature even in bulk state.

Magnetization hysteresis loops of the composites samples are symmetrical (single loop) in nature, and moreover their magnetizations fall in between the magnetizations of CFO and NFO samples that signifies a proper magnetic exchange interactions between two phases (hard and soft magnetic phases) through exchange-spring mechanism.

As CFO content increases in the composite, both saturation magnetization and anisotropy constant found to be increased; this is because the magnetization and anisotropy of CFO sample are higher than that of the NFO sample. Interestingly, the composite with 50NFO +50CFO

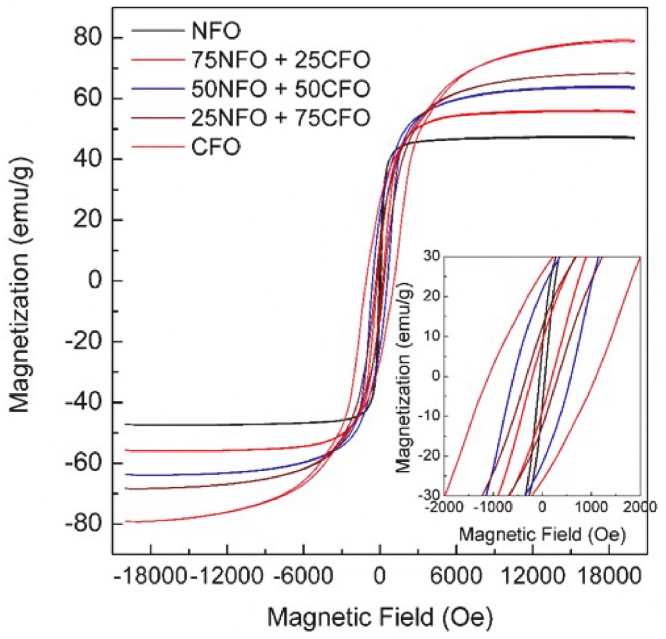

Fig. 6. Magnetization loops of the sintered NFO, CFO and their composites samples.

sample shows higher H_C and M_r than the values found for other two composites.

Magnetic phase transition temperatures (Curie temperature, T_C) of the sintered NFO, CFO and 50NFO + 50CFO composite samples were determined by recording their thermomagnetic (M *vs* T) curves at a constant magnetic field 100 Oe. The obtained curves are shown in Fig. 8. At low temperatures ($T \leq 250$ °C), both NFO and CFO illustrate diverse magnetic behavior, which is due to their soft and hard magnetic features, respectively. In case of NFO sample, magnetization is higher at lower temperature, and it decreases steadily with increment of temperature and drops to zero at a specific temperature (phase transition temperature, $T_C = 591$ °C). This feature certainly defines the soft magnetic and low anisotropic nature of the NFO sample. However, in the CFO case, the magnetization is fairly low at a starting temperature and increases sluggishly up to 250 °C. For $T > 250$ °C, the magnetization rises rapidly to a maximum (peak magnetization) value before it drops to zero. This effect is known as Hopkinson effect and the peak magnetization is called Hopkinson peak, normally observed for hard magnetic and highly anisotropic ferro/ferri magnetic materials such as CFO and Ba- or Sr-hexaferrite systems [48]. The rapid decrease in the anisotropy field (H_a) with temperatue is the prime reason for Hopkinson peak observed in case of CFO sample. The T_C values found for the CFO (521 °C) and NFO (591 °C) samples are concordance with the values often reported for sintered samples [22,26]. For the 50NFO+ 50CFO composite sample, the magnetization at lower temperatures and the T_C (547 °C) lie in-between the values of CFO and NFO samples, indicting existence of both hard and soft magnetic feature in the composite sample. The existence of Hopkinson peak in the 5NFO+ 50CFO composite sample signifies the presence of CFO phase in the composite, despite the composite powder heated at elevated temperature.

3.2.4. Magnetostriction characteristics

Magnetostriction strain (λ) curves of the sintered CFO, NFO and their composites are shown in Fig. 9. These curves were obtained by the

Table 3
Magnetic parameters of sintered samples.

Sample	M_s (emu/g) (±1)	M @ 20 kOe (emu/g) (±1)	H_c (Oe) (±1)	M_r (emu/g) (±1)	$k_1 \times 10^6$ (erg/cm^3) (0.01×10^6)	T_C (°C) (±1)
NFO	47	48	56	7	0.8	591
75NFO + 25CFO	56	56	203	9	1.1	–
50NFO+ 50CFO	64	64	584	22	1.98	547
25NFO+ 75CFO	69	68	324	13	2.72	–
CFO	81	79	1094	26	4.44	521

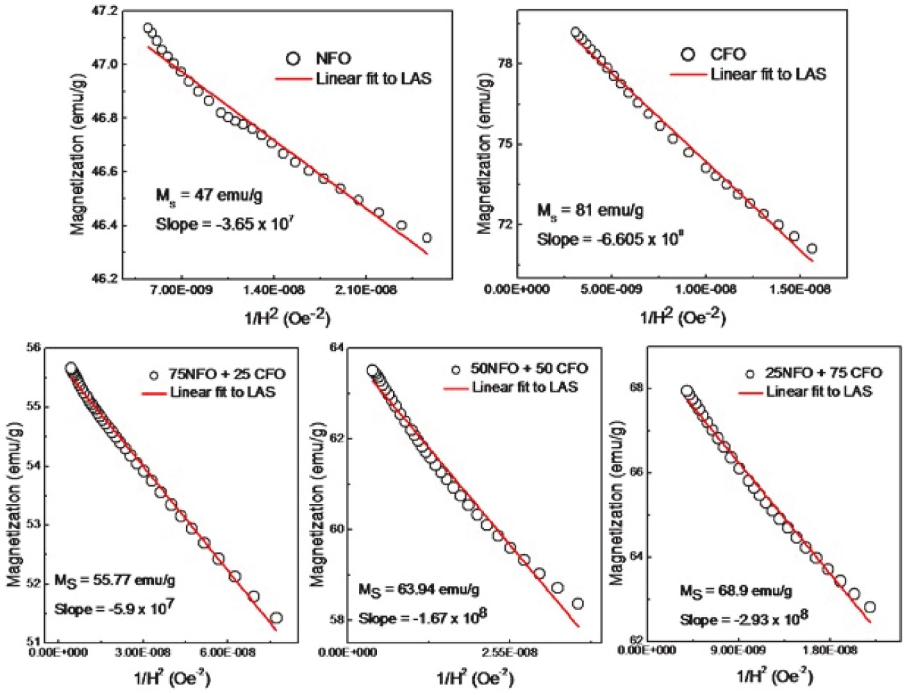

Fig. 7. High-field M vs $1/H^2$ data of the samples fitted with linear function to extract M_S and K_1 values.

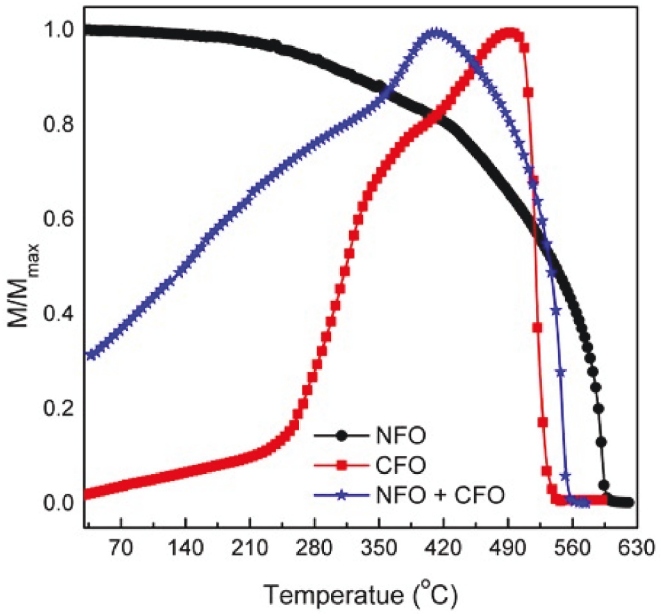

Fig. 8. Magnetization curves of NFO ($NiFe_2O_4$), CFO ($CoFe_2O_4$) and the 50NFO + 50CFO composite samples measured as a function of temperature at a constant magnetic field (100 Oe).

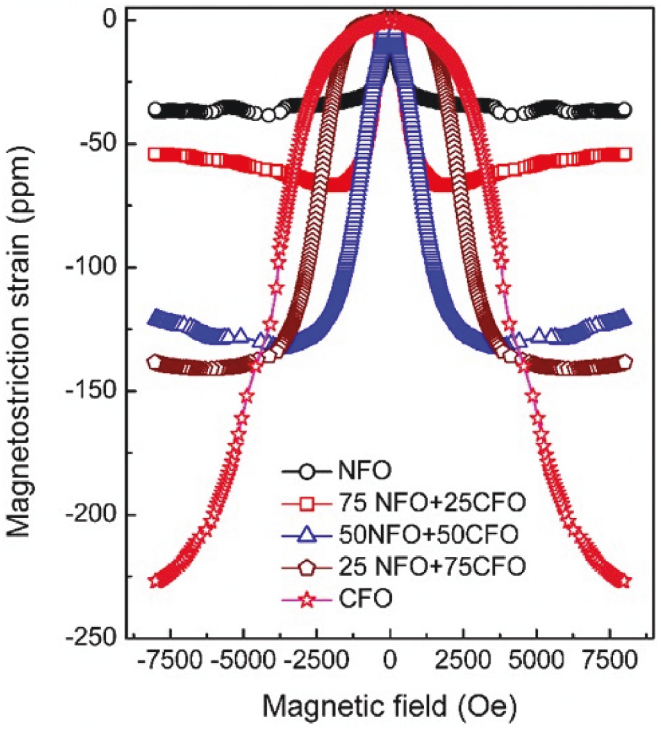

Fig. 9. Magnetostriction strain ($\lambda_{||}$) curves of sintered CFO, NFO and their composites samples, measured at room temperature using 350 Ω strain gauge along the field direction.

measurements at ~30 °C along the direction parallel (strain gauge axis direction) to the lines of magnetic field. As expected, both CFO and NFO samples show (Fig. 9) negative magnetostriction strain along the field direction (-$\lambda_{||}$), but their magnitudes are different. For CFO, magnetostriction is more or less remains the same (~−4 ppm) up to an applied magnetic field of 1 kOe. At fields >1 kOe, the magnetostriction increases almost steadily with the applied magnetic field and finally attains near saturation at 8 kOe. Since CFO is hard magnetic phase, high strength of magnetic field is indispensable to orient the magnetic domains along the direction of field applied and hence the low magnetostriction at low fields. Maximum magnetostriction strain (λ_{max}) obtained for CFO sample is ~ -225 ppm at highest measuring field (8 kOe) in this study. In general, CFO has two magnetostriction coefficients along two crystallographic directions (λ_{100} (easy-axis) and λ_{111} (hard axis)) [49]. At low fields, λ_{100} dominates and has a negative slope. Whereas at high fields, the contribution of λ_{111} (slope is positive) is significant. It can be seen from Fig. 8 that, even at 8 kOe field (highest measuring field), λ is not attaining the saturation limit of the sample that suggests still the λ_{100} is contributing to the overall magnetostriction of the sample. One of the possible reasons for not having saturation magnetostriction in CFO case is smaller grain size (less than 1 μm); smaller the grain size higher the anisotropy and therefore high field strength is required to surmount the same.

Unlike CFO, magnetostriction of NFO attains saturation even at lower magnetic field (λ_{max} = ~-33 ppm at 1.5 kOe) and thereafter the magnetostriction is more or less remains the same. Higher magnetostriction at lower magnetic fields certainly signifies soft magnetic and low anisotropic features of NFO sample. The λ_{max} of NFO sample obtained in the present study is unanimous with the values often reported for the sintered NFO systems [22,23].

Similar to the magnetization loops of the sintered composites, the magnetostriction curves of the sintered composites are also symmetrical in nature owing to proper magnetic exchange interactions between two phases. Like the values of M_S, the λ_{max} values of the sintered composites fall in between the values of CFO and NFO samples. As the CFO content increases in the composite, the magnetostriction strain also increases, due to increase in the magnetocrystalline anisotropy. The values of the λ_{max} and the magnetic field at which those values obtained for CFO, NFO and their composites are listed in Table 4. Although the λ_{max} of composites is lower than that of the CFO sample, at lower magnetic fields the composites show better magnetostriction than the CFO sample.

The values of magnetostriction strain found at lower magnetic fields (500, 1000, 1500 and 2000) for CFO, NFO and their composites are illustrated in Fig. 10. It is evident from Fig. 10 that among all the samples the composite made of 50 wt%NFO and 50 wt%CFO shows better magnetostriction at lower magnetic fields. For instance, at applied magnetic field of 2 kOe, the obtained magnetostriction value for 50NFO+ 50CFO composite is ~ -120 ppm against the values ~ -20 ppm for CFO and ~-30 ppm for NFO. These values indicate nearly 500% enhancement compared to CFO (hard-phase) while nearly 300% higher compared to NFO (soft-phase). The enhanced magnetostriction strain at lower magnetic fields after making composites between soft magnetostriction phase (NFO) and hard magnetostriction phase (CFO) can be ascribed to synergistic effect (exchange-spring mechanism) of both phases. Interface of CFO and NFO phases plays a vital role in mimicking the composite properties. At the interface, the magnetic spins of two phases are strongly coupled through exchange spring mechanism, and as a result of spin coupling it is easier for applied magnetic field to orient the coupled spins (magnetic moments) along the field direction. Hence, the composites (75NFO + 25CFO and 50NFO + 50CFO) display superior magnetostriction strain at lower applied magnetic fields. Notably, as these composites sintered at high temperature, a few of the cations (Ni,

Table 4
λ_{max} and the field at which λ_{max} obtained for sintered NFO, CFO and their composites.

Sample	λ_{max} (ppm) (±3)	H @ λ_{max} (Oe) (±2)
CFO	−225	8000
75 CFO + 25 NFO	−142	5340
50 CFO + 50 NFO	−135	3364
25 CFO + 75 NFO	−65	1820
NFO	−33	1500

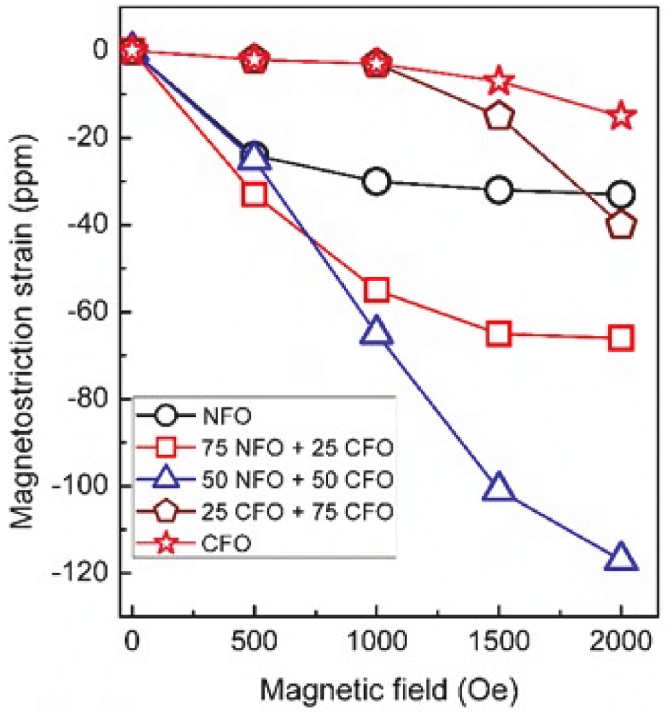

Fig. 10. Magnetostriction strain values found for NFO, CFO and their composites at low magnetic fields (0.5, 1, 1.5 and 2 kOe).

Co and Fe) of two phases are likely to be exchanged at the interface and making the system to act distinctly from their components. Similar features were reported for various composite interfaces [16,33,34,50]. Unlike the magnetostriction of CFO (hard-phase), the magnetostriction of 75NFO+ 25CFO and 50NFO+ 50CFO composites increases almost linearly from the starting point and reaches a saturation at a specific magnetic field. After that, the sign of the magnetostriction changes from negative to positive. This is due to the contribution of λ_{111} coefficient at higher magnetic field. Even though the microstructures of composites are comparable to that of CFO, appearance of both λ_{100} (at low fields) and λ_{111} (at high fields) coefficients in the magnetostriction curve of the 75NFO+ 25CFO and 50NFO+ 50CFO composites clearly indicates a strong magnetic coupling between the hard and soft magnetic phases. Thus, the magnetic and magnetostriction measurements validate that the 50NFO+ 50CFO composite can be a suitable material for magnetostriction applications over the individual component CFO and NFO, owing to its higher magnetostriction values at lower magnetic fields as well as higher Curie temperature.

The present study evidently demonstrates an approach to enhance the magnetostriction at lower magnetic fields by making a composite between NFO and CFO through the concept of exchange-spring mechanism, where no need for special processing and/or metal ion substitution into CFO or NFO. Also, comparing to the previous efforts based on making a composite of structurally two different material systems, the CFO + NFO composites being derived from the simple and the family of isostructural and composition-equivalent spinel structured metal-ferrites (MFe_2O_4) may open up new avenues to design materials for electromagnetic device applications.

4. Conclusions

We performed a comprehensive study of the as-synthesized and sintered CFO, NFO nanomaterials and their nanocomposites. All these materials, which are synthesized using a simple, eco-friendly wet chemical (autocombustion method), crystallize in the expected spinel cubic structure that is common to the family of MFe_2O_4 ferrites. The average crystallite sizes of nanocrystalline CFO and NFO are 73 nm and 69 nm, respectively. Magnetic measurements confirm hard magnetic nature of CFO while NFO is soft magnetic. The sintered CFO, NFO and CFO + NFO composites were structurally stable and retain the phase purity. The structure and microstructure studies demonstrate that both phases coexists as a single-phase in the nanocomposite, where the lattice parameter lies in between that of CFO and NFO. The microstructure is characterized by the presence of nearly spherical shape grains with an average size of 670, 550, and 560 nm, respectively, for CFO, NFO, and 50CFO+ 50NFO composites, respectively. The symmetric nature of the magnetization loop confirms the proper exchange coupling between two magnetic phases in the CFO + NFO composites. The magnetic parameters, such as M_S, H_C, K_1 and T_C, of CFO + NFO composite are in between the values of CFO and NFO. The composites exhibit better magnetostriction at lower magnetic fields than the CFO and NFO sintered materials. At an applied magnetic fields of 2 kOe, the magnetostriction 50NFO+ 50CFO composite enhanced by nearly 500% compared to CFO while nearly 300% enhancement seen compared to NFO. The current study clearly indicates a method for improving magnetostriction at lower magnetic fields by combining NFO and CFO using the exchange-spring mechanism, which eliminates the need for additional processing or metal ion replacement in either CFO or NFO. Additionally, the CFO + NFO composite, which is derived from the simple and family of isostructural and composition-equivalent spinel structured metal-ferrites (MFe_2O_4), may open up new avenues for designing materials for electromagnetic device applications when compared to earlier efforts based on creating a composite of structurally two different material systems.

Declaration of competing interest

The authors declare that they have no known competing financial interests or personal relationships that could have appeared to influence the work reported in this paper.

Acknowledgements

P. N. Anantharamaiah is indebted to the Science and Engineering Research Board (SERB), Department of Science and Technology (DST), Govt. of India, for the financial support through the sanction order number, CRG/2018/002925. The authors (CVR) at the University of Texas at El Paso also acknowledge, with pleasure, support from the National Science Foundation (NSF) with NSF-PREM grant #DMR-1827745.

References

[1] Y. Slimani, M.A. Almessiere, S. Guner, B. Aktas, S.E. Shirsath, M.V. Silibin, A. V. Trukhanov, A. Baykal, Impact of Sm^{3+} and Er^{3+} cations on the structural, optical, and magnetic traits of spinel cobalt ferrite nanoparticles: comparison investigation, ACS Omega 7 (2022) 6292–6301, https://doi.org/10.1021/acsomega.1c06898.

[2] K.K. Bharathi, G. Markandeyulu, C.V. Ramana, structural, magnetic, electrical, and magnetoelectric properties of Sm- and Ho-substituted nickel ferrites, J. Phys. Chem. C 115 (2011) 554–560, https://doi.org/10.1021/jp1060864.

[3] N. Bhalla, S. Taneja, P. Thakur, P.K. Sharma, D. Mariotti, C. Maddi, O. Ivanova, D. Petrov, A. Sukhachev, I.S. Edelman, A. Thakur, Doping independent work function and stable band gap of spinel ferrites with tunable plasmonic and magnetic properties, Nano Lett. 21 (2021) 9780–9788, https://doi.org/10.1021/acs.nanolett.1c03767.

[4] P.N. Anantharamaiah, B.P. Rao, H.M. Shashanka, V. Khopkar, J.A. Chelvane, B. Sahoo, C.V. Ramana, Tunable dielectric properties of nickel ferrite derived via crystallographic site preferential cation substitution, J. Phys. Chem. C 126 (2022) 9123–9134, https://doi.org/10.1021/acs.jpcc.2c00529.

[5] S.M. Ansari, B.B. Sinha, D. Phase, D. Sen, P.U. Sastry, Y.D. Kolekar, C.V. Ramana, Particle size, morphology, and chemical composition controlled $CoFe_2O_4$ nanoparticles with tunable magnetic properties via oleic acid based solvothermal synthesis for application in electronic devices, ACS Appl. Nano Mater. 2 (2019) 1828–1843, https://doi.org/10.1021/acsanm.8b02009.

[6] N. Zufelato, V.R. Aquino, N. Shrivastava, S. Mendanha, R. Miotto, A.F. Bakuzis, Heat generation in magnetic hyperthermia by manganese ferrite-based

nanoparticles arises from Néel collective magnetic relaxation, ACS Appl. Nano Mater. 5 (2022) 7521–7539, https://doi.org/10.1021/acsanm.2c01536.
[7] P. Guo, Y. Zhang, F. Han, Y. Du, B. Song, W. Wang, X. Wang, Y. Zhou, P. Xu, Unveiling the coercivity-induced electrocatalytic oxygen evolution activity of single-domain $CoFe_2O_4$ nanocrystals under a magnetic field, J. Phys. Chem. Lett. 13 (2022) 7476–7482, https://doi.org/10.1021/acs.jpclett.2c01843.
[8] M. Harada, M. Kuwa, R. Sato, T. Teranishi, M. Takahashi, S. Maenosono, Cation distribution in monodispersed MFe_2O_4 (M= Mn, Fe, Co, Ni, and Zn) nanoparticles investigated by X-ray absorption fine structure spectroscopy: implications for magnetic data storage, catalysts, sensors, and ferrofluids, ACS Appl. Nano Mater. 3 (2020) 8389–8402, https://doi.org/10.1021/acsanm.0c01810.
[9] M.M. Khan, W. Khan, M. Ahamed, J. Ahmed, M.A. Al-Gawati, A.N. Alhazaa, Silver-decorated cobalt ferrite nanoparticles anchored onto the graphene sheets as electrode materials for electrochemical and photocatalytic applications, ACS Omega 5 (2020) 31076–31084, https://doi.org/10.1021/acsomega.0c04191.
[10] B. Debnath, H.G. Salunke, S. Bhattacharyya, Spin disorder and particle size effects in cobalt ferrite nanoparticles with unidirectional anisotropy and permanent magnet-like characteristics, J. Phys. Chem. C 124 (2020) 25992–26000, https://doi.org/10.1021/acs.jpcc.0c07382.
[11] S. Biswas, S.S. Panja, S. Bose, Physical insight into the mechanism of electromagnetic shielding in polymer nanocomposites containing multiwalled carbon nanotubes and inverse-spinel ferrites, J. Phys. Chem. C 122 (2018) 19425–19437, https://doi.org/10.1021/acs.jpcc.8b05867.
[12] J.C. Slonczewski, Anisotropy and magnetostriction in magnetic oxides, J. Appl. Phys. 32 (1961) S253, https://doi.org/10.1063/1.2000425.
[13] B.G. Toksha, S.E. Shirsath, S.M. Patange, K.M. Jadhav, Structural investigations and magnetic properties of cobalt ferrite nanoparticles prepared by sol–gel auto combustion method, Solid State Commun. 147 (2008) 479–483, https://doi.org/10.1016/j.ssc.2008.06.040.
[14] S.S. Jadhav, S.E. Shirsath, S.M. Patange, K.M. Jadhav, Effect of Zn substitution on magnetic properties of nanocrystalline cobalt ferrite, J. Appl. Phys. 108 (2010), 093920, https://doi.org/10.1063/1.3499346.
[15] S.E. Shirsath, X. Liu, Y. Yasukawa, S. Li, A. Morisako, Switching of magnetic easy-axis using crystal orientation for large perpendicular coercivity in $CoFe_2O_4$ thin film, Sci. Rep. 6 (2016) 1–11, https://doi.org/10.1038/srep30074.
[16] S.E. Shirsath, C. Cazorla, T. Lu, L. Zhang, Y.Y. Tay, X. Lou, Y. Liu, S. Li, D. Wang, Interface-charge induced giant electrocaloric effect in lead free ferroelectric thin-film bilayers, Nano Lett. 20 (2019) 1262–1271, https://doi.org/10.1021/acs.nanolett.9b04727.
[17] S.E. Shirsath, D. Wang, J. Zhang, A. Morisako, S. Li, X. Liu, Single-crystal-like textured growth of $CoFe_2O_4$ Thin Film on an amorphous substrate: a self-bilayer approach, ACS Appl. Electron. Mater. 2 (2020) 3650–3657, https://doi.org/10.1021/acsaelm.0c00716.
[18] I.C. Nlebedim, N. Ranvah, P.I. Williams, Y. Melikhov, F. Anayi, J.E. Snyder, A. J. Moses, D.C. Jiles, Influence of vacuum sintering on microstructure and magnetic properties of magnetostrictive cobalt ferrite, J. Magn. Magn Mater. 321 (2009) 2528–2532, https://doi.org/10.1016/j.jmmm.2009.03.021.
[19] K.K. Mohaideen, P.A. Joy, Enhancement in the magnetostriction of sintered cobalt ferrite by making self-composites from nanocrystalline and bulk powders, ACS Appl. Mater. Interfaces 4 (2012) 6421–6425, https://doi.org/10.1021/am302053q.
[20] K.K. Mohaideen, P.A. Joy, High magnetostriction and coupling coefficient for sintered cobalt ferrite derived from superparamagnetic nanoparticles, Appl. Phys. Lett. 101 (2012), 072405, https://doi.org/10.1063/1.4745922.
[21] K.K. Mohaideen, P.A. Joy, Influence of initial particle size on the magnetostriction of sintered cobalt ferrite derived from nanocrystalline powders, J. Magn. Magn Mater. 346 (2013) 96–102, https://doi.org/10.1016/j.jmmm.2013.07.016.
[22] P.N. Anantharamaiah, B.P. Rao, H.M. Shashanka, J.A. Chelvane, V. Khopkar, B. Sahoo, Role of Mg^{2+} and In^{3+} substitution on magnetic, magnetostrictive and dielectric properties of $NiFe_2O_4$ ceramics derived from nanopowders, Phys. Chem. Chem. Phys. 23 (2021) 1694–1705, https://doi.org/10.1039/D0CP05448H.
[23] M. Atif, M. Nadeem, R. Grössinger, R.S. Turtelli, Studies on the magnetic, magnetostrictive and electrical properties of sol–gel synthesized Zn doped nickel ferrite, J. Alloys Compd. 509 (2011) 5720–5724, https://doi.org/10.1016/j.jallcom.2011.02.163.
[24] P. Martins, Y.V. Kolenko, J. Rivas, S. Lanceros-Mendez, Tailored magnetic and magnetoelectric responses of polymer-based composites, ACS Appl. Mater. Interfaces. 7 (2015) 15017–15022, https://doi.org/10.1021/acsami.5b04102.
[25] M. Zeng, J.G. Wan, Y. Wang, H. Yu, J.M. Liu, X.P. Jiang, C.W. Nan, Resonance magnetoelectric effect in bulk composites of lead zirconatetitanate and nickel ferrite, J. Appl. Phys. 95 (2004) 8069–8073, https://doi.org/10.1063/1.1739531.
[26] P.N. Anantharamaiah, H.M. Shashanka, S. Saha, J.A. Chelvane, B. Sahoo, Enabling cobalt ferrite ($CoFe_2O_4$) for low magnetic field strain responsivity through Bi^{3+} substitution: material for magnetostrictive sensors, J. Alloys Compd. 877 (2021), 160285, https://doi.org/10.1016/j.jallcom.2021.160285.
[27] P.N. Anantharamaiah, P.A. Joy, Effect of size and site preference of trivalent non-magnetic metal ions (Al^{3+}, Ga^{3+}, In^{3+}) substituted for Fe^{3+} on the magnetostrictive properties of sintered $CoFe_2O_4$, J. Phys. D Appl. Phys. 50 (2017), 435005, https://doi.org/10.1088/1361-6463/aa8af6.
[28] J.A. Paulsen, A.P. Ring, C.C.H. Lo, J.E. Snyder, D.C. Jiles, Manganese-substituted cobalt ferrite magnetostrictive materials for magnetic stress sensor applications, J. Appl. Phys. 97 (2005), 044502. https://aip.scitation.org/doi/abs/10.1063/1.1839633.
[29] P.N. Anantharamaiah, H.M. Shashanka, R. Kumar, J.A. Chelvane, B. Sahoo, Chemically enabling $CoFe_2O_4$ for magnetostrictive strain sensing applications at lower magnetic fields: effect of Zn substitution, Mater. Sci. Eng. B 266 (2021), 115080, https://doi.org/10.1016/j.mseb.2021.115080.
[30] P.N. Anantharamaiah, P.A. Joy, Large enhancement in the magnetostriction parameters of the composite of $CoFe_2O_4$ and $CoFe_{1.9}Ga_{0.1}O_4$, Mater. Lett. 236 (2019) 303–306, https://doi.org/10.1016/j.matlet.2018.10.115.
[31] P.N. Anantharamaiah, P.A. Joy, Enhancing the strain sensitivity of $CoFe_2O_4$ at low magnetic fields without affecting the magnetostriction coefficient by substitution of small amounts of Mg for Fe, Phys. Chem. Chem. Phys. 18 (2016) 10516–10527, https://doi.org/10.1039/C6CP00369A.
[32] E.F. Kneller, R. Hawig, The exchange-spring magnet: a new material principle for permanent magnets, IEEE Trans. Magn. 27 (1991), https://doi.org/10.1109/20.102931, 3588-3560.
[33] D. Roy, P.S.A. Kumar, Enhancement of $(BH)_{max}$ in a hard-soft-ferrite nanocomposite using exchange spring mechanism, J. Appl. Phys. 106 (2009), 073902, https://doi.org/10.1063/1.3213341.
[34] D. Roy, P.S.A. Kumar, Exchange spring behaviour in $SrFe_{12}O_{19}$-$CoFe_2O_4$ nanocomposites, AIP Adv. 5 (2015), 077137, https://doi.org/10.1063/1.4927150.
[35] S.M. Hoque, C. Srivastava, V. Kumar, N. Venkatesh, H.N. Das, D.K. Saha, K. Chattopadhyay, Exchange-spring mechanism of soft and hard ferrite nanocomposites, Mater. Res. Bull. 48 (2013) 2871–2877, https://doi.org/10.1016/j.materresbull.2013.04.009.
[36] J. Lee, G. Lee, T.Y. Hwang, H.R. Lim, H.B. Cho, J. Kim, Y.H. Choa, Phase-and composition-tunable hard/soft magnetic nanofibers for high-performance permanent magnet, ACS Appl. Nano Mater. 3 (2020) 3244–3251, https://doi.org/10.1021/acsanm.9b02470.
[37] Q. Zeng, D. Jiang, S. Yang, Enhancement of magnetic properties in hard/soft $CoFe_2O_4$/Fe_3O_4 nanocomposites, RSC Adv. 6 (2016) 46143–46148, https://doi.org/10.1039/C6RA02993K.
[38] S. Torkian, A. Ghasemi, Energy product enhancement in sufficiently exchange-coupled nanocomposite ferrites, J. Magn. Magn Mater. 469 (2019) 119–127, https://doi.org/10.1016/j.jmmm.2018.07.018.
[39] M.Z. Khan, H. Abbas, K. Nadeem, A. Iqbal, I.L. Papst, Concentration dependent exchange coupling in $BaFe_{12}O_{19}$/$NiFe_2O_4$ nanocomposites, J. Alloys Compd. 922 (2022), 166105, https://doi.org/10.1016/j.jallcom.2022.166105.
[40] R. Safi, A. Ghasemi, R. Shoja-Razavi, The role of shell thickness on the exchange spring mechanism of cobalt ferrite/iron cobalt magnetic nanocomposites, Ceram. Int. 43 (2017) 617–624, https://doi.org/10.1016/j.ceramint.2016.09.203.
[41] S.E. Shirsath, D. Wang, S.S. Jadhav, M.L. Mane, S. Li, in: L. Klein, M. Aparicio, A. Jitianu (Eds.), Ferrites Obtained by Sol-Gel Method, Handbook of Sol-Gel Science and Technology, Springer, New York, 2018, pp. 695–735.
[42] C.V. Ramana, K. Kamala Bharathi, A. Garcia, A.L. Campbell, Growth behavior, lattice expansion, strain, and surface morphology of nanocrystalline, monoclinic HfO_2 thin films, J. Phys. Chem. C 116 (2012) 9955–9960, https://doi.org/10.1021/jp211109h.
[43] S.M. Ansari, R.D. Bhor, K.R. Pai, S. Mazumder, D. Sen, Y.D. Kolekar, C.V. Ramana, Size and chemistry controlled cobalt-ferrite nanoparticles and their anti-proliferative effect against the MCF-7 breast cancer cells, ACS Biomater. Sci. Eng. 2 (2016) 2139–2152, https://doi.org/10.1021/acsbiomaterials.6b00333.
[44] G.K. Williamson, W.H. Hall, X-ray line broadening from filed aluminium and wolfram, Acta Metall. 1 (1953) 22–31, https://doi.org/10.1016/0001-6160(53)90006-6.
[45] B.D. Cullity, Elements of X-Ray Diffraction, second ed., Notre Dame, Indiana, 1977.
[46] A. Franco Jr., F.C. e Silva, High temperature magnetic properties of cobalt ferrite nanoparticles, Appl. Phys. Lett. 96 (2010), 172505, https://doi.org/10.1063/1.3422478.
[47] T.P. Poudel, B.K. Rai, S. Yoon, D. Guragain, D. Neupane, S.R. Mishra, The effect of gadolinium substitution in inverse spinel nickel ferrite: structural, Magnetic, and Mössbauer study, J. Alloys Compd. 802 (2019) 609–619, https://doi.org/10.1016/j.jallcom.2019.06.201.
[48] P.A. Joy, S.K. Date, Effect of sample shape on the zero-field-cooled magnetization behavior: comparative studies on $NiFe_2O_4$, $CoFe_2O_4$ and $SrFe_{12}O_{19}$, J. Magn. Magn Mater. 222 (2000) 33–38, https://doi.org/10.1016/S0304-8853(00)00572-2.
[49] P.N. Anantharamaiah, P.A. Joy, Magnetic and magnetostrictive properties of aluminium substituted cobalt ferrite synthesized by citrate-gel method, J. Mater. Sci. 50 (2015) 6510–6517, https://doi.org/10.1007/s10853-015-9211-x.
[50] S.E. Shirsath, M.H.N. Assadi, J. Zhang, N. Kumar, A.S. Gaikwad, J. Yang, H. E. Maynard-Casely, Y.Y. Tay, J. Du, H. Wang, Y. Yao, Interface-driven multiferroicity in cubic $BaTiO_3$-$SrTiO_3$ Nanocomposites, ACS Nano 16 (2022) 15413–15424, https://doi.org/10.1021/acsnano.2c07215.